JOURNAL OF COMPUTATIONAL PHYSICS 117, 146–162 (1995)

A New Algorithm with Plane Waves and Wavelets for Random Velocity Fields with Many Spatial Scales

FRANK W. ELLIOTT, JR.*‡

Program in Applied and Computational Mathematics, Princeton University, Princeton, New Jersey 08544

AND

ANDREW J. MAJDA†‡

Department of Mathematics and Program in Applied and Computational Mathematics, Princeton University, Princeton, New Jersey 08544

Received May 9, 1994; revised August 31, 1994

A new Monte Carlo algorithm for constructing and sampling stationary isotropic Gaussian random fields with power-law energy spectrum, infrared divergence, and fractal self-similar scaling is developed here. The theoretical basis for this algorithm involves the fact that such a random field is well approximated by a superposition of random one-dimensional plane waves involving a fixed finite number of directions. In general each one-dimensional plane wave is the sum of a random shear layer and a random acoustical wave. These one-dimensional random plane waves are then simulated by a wavelet Monte Carlo method for a single space variable developed recently by the authors. The computational results reported in this paper demonstrate remarkable low variance and economical representation of such Gaussian random fields through this new algorithm. In particular, the velocity structure function for an imcompressible isotropic Gaussian random field in two space dimensions with the Kolmogoroff spectrum can be simulated *accurately over* 12 *decades* with *only* 100 realizations of the algorithm with the scaling exponent accurate to 1.1% and the constant prefactor accurate to 6%; in fact, the exponent of the velocity structure function can be computed over 12 decades within 3.3% with only 10 realizations. Furthermore, only 46,592 active computational elements are utilized in each realization to achieve these results for 12 decades of scaling behavior.

INTRODUCTION

In this paper a new Monte Carlo algorithm is developed for simulating random velocity fields with many spatial scales and an infrared divergent power law spectrum. Generating such random velocity fields with many scales accurately, efficiently, and with low variance is an important and challenging problem in diverse applications such as turbulent diffusion [1–3], solute transport in ground water [4], turbulent combustion [5], and random topography in statistical physics [6].

An important prototype application of this sort involves the accurate generation of a stationary, homogeneous, isotropic, incompressible, mean zero, Gaussian random field with infrared divergence in d-space dimensions such as the Kolmogoroff spectrum [1, 2]. A Gaussian random field, $\mathbf{v}(x)$, with these properties is completely characterized by its two-point correlation matrix [7] which has the form

$$\langle \mathbf{v}(x+x') \otimes \mathbf{v}(x') \rangle = \lim_{\delta \to 0} V^2 \int_{|\mathbf{k}|<\delta} e^{2\pi i x \cdot \mathbf{k}} \frac{|\mathbf{k}|^{1-\varepsilon-d+1}}{2A_d} P(\mathbf{k}) d\mathbf{k}, \quad (1)$$

where $P(\mathbf{k})$ is the matrix projection on the incompressible flows at wave number $\mathbf{k}$ given by

$$P(\mathbf{k}) = I - \frac{\mathbf{k} \otimes \mathbf{k}}{|\mathbf{k}|^2}, \quad (2)$$

where V^2 is a constant and A_d is the area of the unit sphere in R^d. In standard fashion, the notation $\otimes$ denotes the tensor product of vectors. The random field in (1) needs to be interpreted in a generalized sense (see [8]) because

$$\begin{aligned} &\text{for the parameter range, } 2 < \varepsilon < 4, \\ &\text{there is infrared divergence of energy since} \\ &\langle |\mathbf{v}|^2(x) \rangle \to \infty \text{ as } \delta \to 0. \end{aligned} \quad (3)$$

Despite this infrared divergence, the velocity structure function remains finite and is given by

* Research supported by Grant DARPA N00014-92-J-1796.

† Research partially supported by Grants ARO DAAL 03-92-G-0010, DARPA N00014-92-J-1796, ONR N00014-89-J-1044, P00003, NSF DMS-99301094.

‡ Supercomputer support provided by Pittsburgh Supercomputer Center.

0021-9991/95 $6.00

$$\langle |\mathbf{v}(x+x') - \mathbf{v}(x')|^2 \rangle = C_\varepsilon |x|^{\varepsilon-2} \text{ for } 2 < \varepsilon < 4. \quad (4)$$

In (1) and (4), the value $\varepsilon = \frac{8}{3}$ corresponds to the famous $\frac{5}{3}$ law for the Kolmogoroff spectrum in d-space dimensions or the $\frac{2}{3}$ scaling law in physical space [1, 2]. With (4) it follows that almost every realization of the Gaussian random field in (1) is a nowhere differentiable self-similar fractal field [6, 9].

In the numerical results reported in Section 4 of this paper, the authors demonstrate that the *new Monte Carlo algorithm developed* in Sections 2 and 3 of *this paper is capable of simulating accurately the incompressible random velocity field* defined through (1) *in two space dimensions for the Kolmogoroff spectrum over* 12 *decades with remarkably low variance. In fact, the error in the exponent for the velocity structure function in* (4) *with only 10 samples is* 3.3% *over* 12 *decades; with* 100 *realizations, the error in the exponent for the velocity structure function is* 1.1% *over* 12 *decades; furthermore, with* 100 *realizations, even the prefactor in the scaling law for the structure function is computed accurately within* 6% *over the entire* 12 *decades. Nevertheless, only* 46,592 *active elements in each realization are needed to achieve these computational results over the range of* 12 *decades* so there is extremely economical representation through this new algorithm. As reported in Section 4, similar behavior is achieved for more sensitive statistical quantities such as the transverse and longitudinal components of the velocity structure tensor. This performance compares very favorably with standard Fourier representations and/or successive random addition algorithms for these problems which have been reported recently by Viecelli and Canfield [10] to give roughly two decades of scaling in Fourier space with many more realizations required (on the order of several thousand) for these results. Furthermore, the authors, together with D. Horntrop and R. McLaughlin, have recently demonstrated rigorously (see [11]) that even in one space dimension, the popular successive random addition algorithm ([6]) is inconsistent with (1) and must have errors exceeding 200% in the prefactor in (4) for the Kolmogoroff value, $\varepsilon = \frac{8}{3}$.

The new Monte Carlo methods developed in this paper are based on two theoretical considerations:

(A) A general stationary isotropic Gaussian random velocity field is well approximated by an appropriate superposition of random one-dimensional plane waves involving a fixed finite number of directions on the unit sphere. This fact is developed in a quantitative fashion here so that the ensemble averaged systematic errors can be controlled through one preliminary quadrature approximation to a deterministic function (32 directions for an incompressible field with the Kolmogoroff value, $\varepsilon = \frac{8}{3}$, and $d = 2$ are sufficient for the numerical computations in Section 4). Furthermore, this approximation is Gaussian, stationary, and incompressible if the original field is incompressible. This procedure has been outlined and utilized recently by one of the authors in theoretical studies for turbulent diffusion [12].

(B) For the case of a power law spectrum with infrared divergence in (1), each of the random one-dimensional plane wave fields has a one-dimensional energy spectrum with infrared divergence given by $2V^2|k|^{1-\varepsilon}$ for $2 < \varepsilon < 4$. The wavelet Monte Carlo algorithm developed recently by the authors [8] for one-dimensional random fields with infrared divergences is applied to the one-dimensional fields arising in the approximation from (A). This one-dimensional algorithm exploits scaling properties of the infrared divergent random field in a systematic controlled fashion through suitable wavelets and has small sampling errors throughout the scaling regime [8].

For the case of incompressible random fields, the step in (A) above involves an approximation by simple shear layers as sketched recently in ref. [12] For the general random field, the step in (A) involves superpositions of random shear layers and random acoustical waves.

The approximations in (A) are developed in detail in Section 2 of this paper. With the preliminary information on stationary isotropic Gaussian random fields in Section 1, the general shear layer approximations for an incompressible random field are defined first in Section 2.1. Theoretical and practical formulas which determine the choice and number of random directions are developed in Section 2.1.1; in particular, these conditions are determined by the quadrature of a fixed nonrandom function and this criterion is developed for power law random fields in Section 2.1.2 and is illustrated in detail for the Kolmogoroff spectrum, $\varepsilon = \frac{8}{3}$, with $d = 2$. The random plane wave construction is generalized to compressible isotropic random fields in Section 2.2. The elementary theoretical modifications of the multiwavelet Monte Carlo method from Ref. [8] for the random plane waves as mentioned in (B) above are developed in Section 2.3. With all of these steps, a complete summary of the theoretical algorithm is given in Section 2.4.

Section 3 of this paper is devoted to an important practical issue. A straightforward implementation of the theoretical algorithm summarized in Section 2.4 for random fields involving 12 decades of scaling as in the numerical results reported in Section 4 would require the storage of between 2^{49} to 2^{50} independent normal Gaussian random variables. Such storage requirements are prohibitive on even the largest supercomputers. In Section 3, the algebra of linear congruential generators for pseudorandom numbers is utilized, together with the structure of the basic algorithm, so that all the random weights in a given calculation (even with 12 decades of active scales!!) require only a small amount of time and memory. Furthermore, the algorithm with this strategy is fully vectorizable. However, Section 3 has a different technical flavor compared with the remainder of the paper and the reader can skip from Section 2.4 directly to the computational results in Section 4 without studying Section 3 and disrupting the main reasoning.

1. STATIONARY GAUSSIAN RANDOM VELOCITY FIELDS

A Gaussian vector field $v(\cdot)$ on $\mathbb{R}^d$ is a random vector field which has jointly Gaussian values on all finite sets of points

of $\mathbb{R}^d$. We assume that the expected value of the field $v(\cdot)$ at each point x is zero; i.e., $v(\cdot)$ has zero mean, and the joint distribution of $v(x + x')$ and $v(x')$ depends only on x; i.e., $v(\cdot)$ is stationary. These two properties are summarized in the equations

$$\langle v(x) \rangle = 0 \tag{5a}$$

$$\langle v(x + x') \otimes v(x') \rangle = R(x) = R(-x), \tag{5b}$$

which determine the joint Gaussian distribution of the values of $v(\cdot)$ at each finite set of points in $\mathbb{R}^d$ (the so-called finite-dimensional distributions of $v(\cdot)$). The tensor $R(\cdot)$ is the *covariance tensor* of the random field $v(\cdot)$. Here and below $\langle \cdot \rangle$ denotes the ensemble average. Since we are interested in infrared divergent velocity fields, we also consider zero mean, stationary, *generalized* Gaussian vector fields; such fields are evaluated by integration with respect to test fields chosen so that the resulting integrals have finite variance. (We refer the interested reader to [8] for discussion and use of such test fields. Here they are omitted for simplicity in exposition.)

For the analysis and synthesis of stationary Gaussian vector fields, the covariance tensor $R(\cdot)$ can be represented in terms of its Fourier transform, the spectral tensor E. The spectral tensor is defined by

$$R(x) = \int_{\mathbb{R}^d} e^{-i2\pi x \cdot k} E(k)\, dk, \tag{6}$$

where we define the Fourier transform $\mathcal{F}$ and the inverse Fourier transform $\mathcal{F}^{-1}$ by

$$(\mathcal{F} f)(k) = \int_{\mathbb{R}^d} e^{i2\pi k \cdot x} f(x)\, dx \tag{7a}$$

$$(\mathcal{F}^{-1} f)(x) = \int_{\mathbb{R}^d} e^{-i2\pi k \cdot x} f(k)\, dk. \tag{7b}$$

for a scalar, vector, or tensor field f. As mentioned in the Introduction, we are particularly interested in fields which have spectra with nonintegrable singularities at $k = 0$, *strong infrared divergences*. Scalar fields of this sort define the typical random functions which are fractal for almost every realization.

2. THE RANDOM PLANE WAVE ALGORITHM

The spectral tensor of a stationary, Gaussian field $v(\cdot)$ can be simplified by using the Helmholtz decomposition, provided that the field is isotropic. This simplification leads to a representation of the field in terms of random plane waves (see [12]). In saying that a field $v(\cdot)$ is isotropic, we mean that for any rotation U with transpose U^*,

$$U^* v(U\cdot) = v(\cdot) \tag{8}$$

in the sense that both fields have the same finite-dimensional distributions. The Helmholtz decomposition of $v(\cdot)$,

$$v(x) = v_1(x) + v_2(x)$$

$$v_1(x) = (\mathcal{F}^{-1} P_1 \mathcal{F} v)(x) \tag{9a}$$

$$v_2(x) = (\mathcal{F}^{-1} P_2 \mathcal{F} v)(x), \tag{9b}$$

resolves $v(\cdot)$ into an irrotational (incompressible) component $v_1(\cdot)$ and a solenoidal (acoustic) component $v_2(\cdot)$. Here P_1 and P_2 are the *transverse* and *longitudinal* matrix projections at each wave number k given by

$$P_1(k) = I - |k|^{-2} k \otimes k \tag{10a}$$

$$P_2(k) = |k|^{-2} k \otimes k. \tag{10b}$$

If $v(\cdot)$ is isotropic, then the spectral tensor has the form

$$E(k) = \frac{1}{2A_d |k|^{d-1}} (E_1(|k|) P_1(k) + E_2(|k|) P_2(k)) \tag{11}$$

(see [7]) so that $v_1(\cdot)$ and $v_2(\cdot)$ are statistically independent. Here, A_d is the area of the unit sphere in $\mathbb{R}^d$, E_1 and E_2 are the transverse and longitudinal radial spectra (scalar even functions). The auto-covariances of the incompressible component $v_1(\cdot)$ and the acoustic component $v_2(\cdot)$ are

$$\begin{aligned} R_{jj}(x) &= \langle v_j(x + x') \otimes v_j(x') \rangle \\ &= \int_{\mathbb{R}^d} e^{i2\pi k \cdot x} \frac{E_j(|k|)}{2A_d |k|^{d-1}} P_j(k)\, dk \\ &= \int_{S^{d-1}} P_j(\omega) \int_0^\infty \cos(2\pi \tilde{k} \omega \cdot x) E_j(\tilde{k})\, d\tilde{k}\, d\omega, \end{aligned} \tag{12}$$

where $j = 1, 2$, the $P_j(\omega)$ are the projections in (10), and S^{d-1} is the unit sphere in $\mathbb{R}^d$; the cross-covariances $R_{12} = R_{21}$ are zero.

2.1. Shear Layer Approximations for Incompressible Fields

Using the auto-covariance formula in (12), we can construct random plane wave fields that have the same first- and second-order statistics as v_1 and v_2 (see [12]). First, we carry out this program for v_1 because our primary interest is in incompressible fluid mechanics. In this case the plane waves are called *shear waves* because the axis of variation of such a wave is perpendicular to the plane in which its components are nonzero and, thus, it defines a shear flow. In this subsection we use arrows, $\mathbf{x}$, to denote elements of $\mathbb{R}^d$ to avoid confusion with scalar variables, $x \in \mathbb{R}^1$.

Let $N(\cdot)$ be *white noise*, which is the scalar generalized Gaussian random process defined by

$$\langle N(x)\rangle = 0 \tag{13a}$$

$$\langle N(x+x') \otimes N(x')\rangle = \delta(x), \tag{13b}$$

where $\delta(\cdot)$ is the Dirac delta function. Let $\{N_s | s = 1, 2, ..., d\}$ be independent white noise processes, and let $\{e_s | s = 1, 2, ..., d\}$ be the standard basis for $\mathbb{R}^d$. Define a stationary Gaussian vector random process in a single space variable with the one-dimensional spectrum $E_1(k)$ from (11) by the *plane wave*

$$\tilde{v}_1(x) = \sum_{s=1}^{d} e_s \int_{-\infty}^{+\infty} (\mathcal{F}^{-1} E_1^{1/2})(x-y) N_s(y)\, dy. \tag{14}$$

The fact that the stationary Gaussian random field in (14) has the spectrum $E_1(k)$ follows from the moving average representation of a Gaussian field. (See [14, 8] for related applications.) Choose the direction $\boldsymbol{\omega}$ at random from a uniform distribution on S^{d-1}. Then, with the projection in (10a) the random shear wave

$$v_1^1(\mathbf{x}) = \left(\frac{A_d}{2}\right)^{1/2} P_1(\boldsymbol{\omega})\tilde{v}_1(\mathbf{x}\cdot\boldsymbol{\omega})$$

is incompressible and has the same mean and covariance as $v_1(\cdot)$ (see [12]); however, $v_1^1(\cdot)$ is only Gaussian if conditioned on the choice of $\boldsymbol{\omega}$. Therefore, we approximate v_1 by standardized sums of independent random shear waves,

$$v_1^M(\mathbf{x}) = \left(\frac{A_d}{2M}\right)^{1/2} \sum_{r=1}^{M} P_1(\boldsymbol{\omega}_r)\tilde{v}_1^r(\mathbf{x}\cdot\boldsymbol{\omega}_r), \tag{15}$$

so that as M goes to infinity v_1^M tends to v_1 by the central limit theorem. With a fixed, finite set of directions, the field in (15) is a stationary, isotropic, incompressible Gaussian random field. Next, in Sections 2.1.1 and 2.1.2 we devise an elementary strategy for choosing these directions involving a preliminary deterministic quadrature.

Analogous formulas hold for general isotropic compressible velocity fields. For the acoustic wave field, $v_2(\mathbf{x})$, we define the one-dimensional random field $v_2(x)$ as in (14) with the acoustical spectrum $E_2(|k|)$ replacing $E_1(|k|)$. Given $v_2(x)$, there is an analogous formula for $v_2^M(x)$ as in (15) involving a finite number of directions, where the acoustical projection $P_2(\omega)$ replaces the incompressible projection $P_1(\omega)$ in (15). This will be discussed in Section 2.2 below.

2.1.1. *Choice of Plane Wave Directions*

In this subsection, we develop explicit, practical formulas for the choice of directions so that the approximating superposition of plane waves is a Gaussian random field. In practice, we choose the directions deterministically. Such approximations have the form

$$v_1^T(x) = \left(\frac{A_d}{2M}\right)^{1/2} \sum_{\omega\in T} P_1(\omega)\tilde{v}_1^{\omega}(x\cdot\omega), \tag{16}$$

where T is a prescribed finite set of M shear directions. (We change notation for the duration of this section to better describe the changes of variables in the shear field representation.) Both the original random field $v_1(\cdot)$ and $v_1^T(\cdot)$ are stationary, incompressible Gaussian fields with mean zero; their covariances are

$$\langle v_1(x+x') \otimes v_1(x')\rangle = R_{11}(x)$$

$$= \int_{S^{d-1}} P_1(\omega)(\mathcal{F}^{-1} E_1)(x\cdot\omega)\, d\omega \tag{17a}$$

$$\langle v_1^T(x+x') \otimes v_1^T(x')\rangle = R_{11}^T(x)$$

$$= \left(\frac{A_d}{2M}\right) \sum_{\omega\in T} P_1(\omega)(\mathcal{F}^{-1} E_1)(x\cdot\omega). \tag{17b}$$

Furthermore, since both random fields are Gaussian, the accuracy of $v_1^T(\cdot)$ as an approximation to $v_1(\cdot)$ is dependent only on the accuracy in approximating the covariance. In general, the formula in (17b) is a finite quadrature approximation to the formula in (17a). We utilize this simple fact in a quantitative strategy in Section 2.1.2.

Besides accurate quadrature, we need to design the directions T to preserve isotropy to high accuracy. Thus, we do a similarity transformation on $R_{11}(x)$ and $R_{11}^T(x)$ so that the former is diagonal; this will allow us to compute formulas for $R_{11}(x)$ so that we can determine the accuracy of $R_{11}^T(x)$ for a given finite set of shear directions T. Let $U(x)$ be the unique rotation which maps $x \in \mathbb{R}^d$ to $|x|e_1$, where e_1 is the first element of the standard basis, while leaving all the vectors perpendicular to x and e_1 invariant. Then,

$$U(x)R_{11}(x)U^*(x) = \int_{S^{d-1}} P_1(\omega)(\mathcal{F}^{-1} E_1)(|x|e_1\cdot\omega)\, d\omega$$

$$= R_{11}(|x|e_1) \tag{18a}$$

$$U(x)R_{11}^T(x)U^*(x) = \left(\frac{A_d}{2M}\right) \sum_{\omega\in U(x)T} P_1(\omega)(\mathcal{F}^{-1} E_1)(|x|e_1\cdot\omega)$$

$$= R_{11}^{U(x)T}(|x|e_1). \tag{18b}$$

A change of coordinates shows that $R_{11}(|x|e_1)$ is diagonal with

$$\begin{aligned} R_{11}(|x|e_1) &= \int_{S^{d-1}} P_1(\omega)(\mathcal{F}^{-1} E_1)(|x|e_1\cdot\omega)\, d\omega \\ &= \int_0^{\pi} H(\theta)(\mathcal{F}^{-1} E_1)(|x|\cos(\theta))\, d\theta, \end{aligned} \tag{19}$$

where

$$\begin{aligned} H(\theta) &= \int_{S^{d-2}} P_1(\cos(\theta)e_1 + \sin(\theta)\boldsymbol{\sigma})\, d\boldsymbol{\sigma} \\ &= A_{d-1}\begin{pmatrix} \sin^2(\theta) & 0 \\ 0 & \left(1 - \dfrac{\sin^2(\theta)}{d-1}\right) I \end{pmatrix}. \end{aligned} \tag{20}$$

2.1.2. *Quadrature Formulas for Power Law Random Fields*

Comparison of $R_{11}(|x|e)$ and $R_{11}^{U(x)T}(|x|e)$ provides a means of bounding the error in $R_{11}^T(x)$ relative to $R_{11}(x)$. If for all rotations U we have the bound

$$\sup_U \frac{\|R_{11}(|x|e_1) - R_{11}^{UT}(|x|e_1)\|}{\|R_{11}(|x|e_1)\|} < \eta \tag{21}$$

for some η much less than 1 and a matrix norm $\|\cdot\|$, e.g.,

$$\|A\| = \left(\sum_{ij} |a_{ij}|^2\right)^{1/2},$$

then

$$\sup_U \frac{\|R_{11}(x) - R_{11}^T(x)\|}{\|R_{11}(x)\|} < \eta, \tag{22}$$

and isotropy is maintained with the tolerance η. If T has M shear directions chosen from an equi-distributed sequence, one would expect η to be $O(1/M)$. For the two-dimensional simulations in this paper, we choose the M shear directions T to be

$$T = \{(\cos(2\pi(k/m)), \sin(2\pi(k/m)))|k = 0, 1, ..., M-1\} \tag{23}$$

so that the elements of T are on the vertices of a regular polygon inscribed in the unit circle. In a subsequent publication we will generalize this construction to three-dimensional random fields.

For the case of a power-law, two-dimensional random field, we have determined error bounds on the number of directions by simple numerical evaluation. As mentioned in (1) to (3) of the Introduction, for an incompressible, power-law random field with $2 < \varepsilon < 4$, the singularity of the radial spectrum $E(k) = 2|k|^{1-\varepsilon}$ is nonintegrable with an infrared divergence so that the covariance tensor is infinite. However, a closely related quantity, the *velocity structure tensor*

$$D_{11}(x) = \langle (v_1(x+x') - v_1(x')) \otimes (v_1(x+x') - v_1(x')) \rangle \tag{24}$$

remains finite. In fact, it follows from (2) that the velocity structure tensor satisfies

$$D_{ll}(x) = |x|^{\varepsilon-2} D_{ll}(x/|x|)$$

and

$$U(x) D_{11}(x) U^*(x) = D_{11}(|x|e_1).$$

For a power-law incompressible random field in d dimensions, the radial spectrum is $E_1(k) = 2|k|^{1-\varepsilon}$. Therefore, with the formula in (20), the value of the velocity structure tensor at $|x|e_1$ is diagonal with two distinct eigenvalues

$$D_{11}(|x|e_1) = |x|^{\varepsilon-2} \begin{pmatrix} \lambda_\parallel(\varepsilon) & 0 \\ 0 & \lambda_\perp(\varepsilon) I \end{pmatrix}, \tag{25}$$

where

$$\lambda_\parallel = A_{d-1} F(1-\varepsilon) B\left(\frac{\varepsilon-1}{2}, \frac{3}{2}\right) \tag{26a}$$

$$\lambda_\perp = A_{d-1} F(1-\varepsilon) \left(B\left(\frac{\varepsilon-1}{2}, \frac{1}{2}\right) - (d-1)^{-1} B\left(\frac{\varepsilon-1}{2}, \frac{3}{2}\right)\right). \tag{26b}$$

Here, $B(\cdot,\cdot)$ is the beta function,

$$B(a,b) = \frac{\Gamma(a)\Gamma(b)}{\Gamma(a+b)},$$

$\Gamma(\cdot)$ is the gamma function defined by the analytic continuation of the integral

$$\Gamma(z) = \int_0^\infty e^{-t} t^{z-1},$$

and $F(z)$ is defined by the analytic continuation of the integral

$$\begin{aligned} F(z) &= 2\int_0^\infty \cos(2\pi k) k^z \, dk \\ &= 2(2\pi)^{-1-z} \cos(2\pi(1+z)) \Gamma(z-1). \end{aligned} \tag{27}$$

For the Kolmogoroff spectrum value with $\varepsilon = \frac{8}{3}$, the structure tensor evaluated at e_1 is

$$D_{11}(e_1) = \begin{pmatrix} 45.984 & 0 \\ 0 & 76.641 \end{pmatrix}$$

to the given accuracy. We denote by $D_{11}^T(e_1)$ the velocity structure tensor of the approximate field $v_1^T(\cdot)$. For spectra with infrared divergence, we replace the isotropic approximation in Eqs. (21) and (22) by the same condition for the velocity structure tensor. Since, in two dimensions the set of all rotations is

$$\{U\} = \left\{ U(\theta) = \begin{pmatrix} \cos(\theta) & \sin(\theta) \\ -\sin(\theta) & \cos(\theta) \end{pmatrix} \middle| 0 \le \theta < 2\pi \right\},$$

the set T is symmetric, and the structure and covariance tensors are proportional, we have

$$\eta = \sup_{\{0 \le \theta < 2\pi/M\}} \frac{\|D_{11}^{U(\theta)T}(e_1) - D_{11}(e_1)\|}{\|D_{11}(e_1)\|}.$$

TABLE I

Isotropy Tolerance for the Velocity Structure Tensor

Shear directions	Quantity	True value	Minimum value	Maximum value	Error percentage
16	d_{11}	45.984	42.370	47.339	7.860
16	d_{12}, d_{21}	0.000	−0.180	0.180	—
16	d_{22}	76.641	76.612	76.674	0.044
16	η				4.044
32	d_{11}	45.984	44.855	46.404	2.457
32	d_{12}, d_{21}	0.000	−0.028	0.028	—
32	d_{22}	76.641	76.639	76.643	0.003
32	η				1.264
64	d_{11}	45.984	45.629	46.116	0.772
64	d_{12}, d_{21}	0.000	−0.004	0.004	—
64	d_{22}	76.641	76.641	76.641	0.000
64	η				0.397

2.1.3. *Deterministic Numerical Quadrature for the Choice of Directions*

Next we present a numerical evaluation of the isotropy factor η. For a given number of shear directions M equal to 16, 32, and 64, Table I compares the range of values of the entries of $D_{11}^{U(\theta)T}(e_1)$ to the entries of $D_{11}(e_1)$ as θ varies from 0 to $2\pi/M$. Table I also gives the absolute percentage error of the entries of the $D_{11}^{U(\theta)T}(e_1)$ with respect to $D_{11}(e_1)$ and the isotropy factor η as a percentage error. We denote the velocity structure tensor $D_{11}^{UT}(e_1)$ of the rotated field elementwise by

$$D_{11}^{UT}(e_1) = \begin{pmatrix} d_{11} & d_{22} \\ d_{21} & d_{22} \end{pmatrix}.$$

Among the entries, the largest errors were made in d_{11}, with an error of 7.86% for 16 shear directions, an error of 2.46% for 32 shear directions, and an error of 0.77% for 64 shear directions. The error in d_{22} was not more than 0.5%. The magnitudes of the off-diagonal entries, d_{12} and d_{21}, were never more than 0.18 in absolute value, which is less than 0.4% of either of the diagonal entries. As a result of all of this the isotropy factor η, discussed earlier in Eqs. (21) and (22), is quite small. For 16 shear directions η is 4.04%, for 32 shear directions η is 1.26%, and for 64 shear directions η is 0.40%.

2.2. Random Plane Waves for Compressible Fields

For applications dealing with compressible velocity fields it is necessary to simulate both the incompressible and the acoustic velocity fields simultaneously. This involves only a minor generalization of the idea developed earlier in detail for the incompressible case. Here we develop in detail the remarks in the last paragraph of Section 2.1. Using the autocovariance formula, (12), we can construct random plane wave fields that have the same first- and second-order statistics as v. With $\tilde{v}_j$, $j = 1, 2$ defined as in (14) with the scalar spectra $E_j(k)$ from (11) we note the trivial statistical identity that

$$U\tilde{v}_j(\cdot) = \tilde{v}_j \tag{28}$$

for $j = 1, 2$. Again in this subsection we use $\mathbf{x}$ to denote an element of $\mathbb{R}^d$ and x to denote a scalar. Recall that $U(\omega)$ is defined as the unique rotation which maps $\omega \in S^{d-1}$ to e_1 and leaves all the vectors perpendicular to ω and e_1 invariant. Thus,

$$P_1(\omega) = U^*(\omega)(I - e_1 \otimes e_1)U(\omega)$$

$$P_2(\omega) = U^*(\omega)(e_1 \otimes e_1)U(\omega),$$

where U^* denotes the transpose of U. Define a stationary Gaussian vector random process on the line by the *plane wave*

$$\tilde{v}(x) = (I - e_1 \otimes e_1)\tilde{v}_1(x) + (e_1 \otimes e_1)\tilde{v}_2(x), \tag{29}$$

and choose ω uniformly on S^{d-1}. Then, we construct the random plane wave $v^1(\mathbf{x})$ with the same mean and covariance as $v(\mathbf{x})$ by

$$\begin{aligned} v^1(\mathbf{x}) &= \left(\frac{A_d}{2}\right)^{1/2} U^*(\omega)\,((I - e_1 \otimes e_1)U(\omega)\tilde{v}_1(\mathbf{x}\cdot\omega) \\ &\quad + (e_1 \otimes e_1)U(\omega)\tilde{v}_2(\mathbf{x}\cdot\omega)) \\ &= \left(\frac{A_d}{2}\right)^{1/2} U^*(\omega)((I - e_1 \otimes e_1)\tilde{v}_1(\mathbf{x}\cdot\omega) \\ &\quad + (e_1 \otimes e_1)\tilde{v}_2(\mathbf{x}\cdot\omega)) \\ &= \left(\frac{A_d}{2}\right)^{1/2} U^*(\omega)\tilde{v}(\mathbf{x}\cdot\omega). \end{aligned}$$

Again, $v^1(\cdot)$ is only Gaussian if conditioned on the choice of ω. Therefore, we approximate v by standardized sums of independent random plane waves

$$v^M(\mathbf{x}) = \left(\frac{A_d}{2M}\right)^{1/2} \sum_{r=1}^{M} U^*(\omega_r)\tilde{v}^r(\mathbf{x}\cdot\omega_r) \tag{30}$$

so that as M goes to infinity v^M tends to v by the central limit theorem. For a precise analysis of the case when the plane wave directions are chosen nonrandomly, one can derive error bounds for the acoustic covariance tensor R_{22}^T for a given choice of plane directions T in the same fashion as we have illustrated above for the incompressible case. The approximation in (30) is a nearly isotropic, stationary Gaussian random field.

2.3. Multiwavelet Monte Carlo Simulation of Plane Waves

With the random field approximation in (16) and more generally (30) via plane waves, an effective Monte Carlo algorithm is needed for random plane waves. Such an algorithm has been developed recently by the authors [8] for the difficult case of power law spectra with infrared divergences. Thus following the procedure in [8], we now represent the plane wave $\tilde{v}(\cdot)$ defined in (29) in terms of its component spectra and expand the white noises defining the plane wave in terms of the Alpert–Rokhlin multiwavelet basis. The expansion is almost identical to the one developed by the authors recently in [8] for a shear wave in two dimensions. Here, we briefly summarize the modifications of that construction which we need. The plane wave $\tilde{v}(\cdot)$ has the spectral tensor

$$\tilde{E}(k) = \begin{pmatrix} E_2(k) & 0 \\ 0 & E_1(k)I \end{pmatrix}$$

so that the components are independent. If G_s is the inverse Fourier transform of the square root of the sth component spectrum of $\tilde{v}(\cdot)$

$$G_s(x) = \begin{cases} (\mathcal{F}^{-1} E_2^{1/2})(x), & \text{if } s = 1 \\ (\mathcal{F}^{-1} E_1^{1/2})(x), & \text{if } 2 \le s \le d, \end{cases} \tag{31}$$

then $\tilde{v}$ can be represented by

$$\tilde{v}(x) = \sum_{s=1}^{d} (G_s * N_s)(x)e_s \tag{32a}$$

$$= \sum_{s=1}^{d} \sum_{m=-\infty}^{+\infty} \sum_{n=-\infty}^{+\infty} \sum_{\sigma=1}^{\tau} (G_s * \phi_{mn}^{\sigma\tau})(x) N_s(\phi_{mn}^{\sigma\tau})e_s. \tag{32b}$$

Here, the star represents the convolution of two functions

$$(f * g)(x) = \int_{-\infty}^{+\infty} f(x-y)g(y)\,dy,$$

and the set $\{N_s | s = 1, 2, ..., d\}$ are independent white noises. In (32b) the set

$$\{\phi_{mn}^{\sigma\tau}(x) | m, n \in Z, \sigma = 1, 2, ..., \tau\}$$

is the Alpert–Rokhlin orthonormal basis (see [15]) for the square integrable functions $L^2(\mathbb{R})$, and the integral of a function with respect to white noise is abbreviated by

$$N(f) = \int_{-\infty}^{+\infty} f(y)N(y)\,dy.$$

By *orthonormal* we mean that the Alpert–Rokhlin basis obeys the condition

$$\int_{-\infty}^{+\infty} \phi_{mn}^{\sigma\tau}(y)\phi_{m'n'}^{\sigma'\tau'}(y)\,dy = \delta_{\sigma}^{\sigma'}\,\delta_{m}^{m'}\,\delta_{n}^{n'} \tag{33}$$

for any two basis elements $\phi_{mn}^{\sigma\tau}$ and $\phi_{m'n'}^{\sigma'\tau'}$, where δ is the Kronecker delta. The Alpert–Rokhlin basis is derived from the set of τ functions

$$\{\phi^{\sigma\tau} | \sigma = 1, 2, ..., \tau\},$$

referred to as the Alpert–Rokhlin *multiwavelet;* the Alpert–Rokhlin multiwavelet functions are piecewise polynomial, are supported only on [0, 1], and were constructed in Ref. [15]. The interested reader can recover all of the facts needed here about the Alpert–Rokhlin basis from the detailed concise summary presented in Ref. [8]. The Alpert–Rokhlin basis is defined as the set of all discrete dilates and translates of the elements of the multiwavelet,

$$\{\phi_{mn}^{\sigma\tau}(x) = 2^{m/2}\,\phi^{\sigma\tau}(2^m x - n) | m, n \in Z, \sigma = 1, 2, ..., \tau\}.$$

Because of its convergence, moment cancellation, and orthonormality properties, the Alpert–Rokhlin basis allows the expansion in (32b) to be represented as a weighted finite sum of standard, independent, and identically distributed Gaussian random variables. When integrated against appropriate test fields (see [8]), the sum over m, the length scale, in (32b) converges so that only a finite number of scales m is required for an approximation of the field $\tilde{v}(\cdot)$. This convergence holds for fields $v(\cdot)$ with integrable spectra as well as for fields with infrared divergences. Moreover, since the Alpert–Rokhlin multiwavelet cancels all moments less than τ, i.e.,

$$\int_{-\infty}^{+\infty} y^q \phi^{\sigma\tau}(y)\,dy = 0$$

for $0 \le q < \tau$, the multiwavelet has the property that the absolute value of the convolution

$$|((\mathcal{F}^{-1} E^{1/2}) * \phi^{\sigma\tau})(x)|,$$

for $\sigma = 1, 2, ..., \tau$, decreases rapidly in $|x|$. (See [8] for a derivation of the rate of decay in the case of the power-law spectrum.) Using these facts about convergence in m, the number of octaves, and n, the translates, we truncate the expansion in (32b) as in [8]. We limit the range of scales m to $m_0 \leq m \leq m_1$, and, at each scale m, we omit those multiwavelets $\phi_{mn}^{\sigma\tau}$ for which the distance from x to the wavelet support $|\lfloor 2^m x \rfloor - n|$ is greater than some threshold b (the bandwidth), where $\lfloor y \rfloor$ denotes the greatest integer less than or equal to y. Therefore, we have

$$\tilde{v}(x) = \sum_{s=1}^{d} \sum_{m=m_0}^{m_1} \sum_{n=\lfloor 2^m x \rfloor - b}^{\lfloor 2^m x \rfloor + b} \sum_{\sigma=1}^{\tau} (G_s * \phi_{mn}^{\sigma\tau})(x) N_s(\phi_{mn}^{\sigma\tau}) e_s. \quad (34)$$

Note that for $2 \leq s \leq d$ all G_s are the same so that the convolutions for the last $d - 1$ components of the plane wave should only be computed once. The orthonormality condition in (33), together with the definition of white noise in (13), imply that the random variables

$$\{N_s(\phi_{mn}^{\sigma\tau}) | m, n \in Z, \sigma = 1, 2, ..., \tau, s = 1, 2, ... d\},$$

which are random weights in (34), are independent and identically distributed Gaussian random variables with mean zero and variance one.

2.4. The Complete Algorithm

Summarizing the theoretical developments in the previous section, we have the following algorithm: The random field $v^T(\mathbf{x})$ approximating the stationary isotropic Gaussian vector field $v(\cdot)$ is given by the formulas

$$v^T(\mathbf{x}) = \sum_{r=1}^{M} U^*(\omega_r) \tilde{v}_r(\mathbf{x} \cdot \omega_r) \quad (35a)$$

$$\tilde{v}_r(x) = \sum_{s=1}^{d} \sum_{m=m_0}^{m_1} \sum_{n=\lfloor 2^m x \rfloor - b}^{\lfloor 2^m x \rfloor + b} \sum_{\sigma=1}^{\tau} (G_s * \phi_{mn}^{\sigma\tau})(x) N_{rs}(\phi_{mn}^{\sigma\tau}) e_s. \quad (35b)$$

As above, $T = \{\omega_r | r = 1, 2, ..., M\}$ is the fixed set of plane wave directions, $U(\omega)$ is the plane rotation which maps ω to e_1, $\{G_s | s = 1, 2, ..., d\}$ is the finite set of coordinate kernels for the plane wave $\tilde{v}$ as defined in (31), and $\{N_{rs} | r = 1, 2, ..., M, s = 1, 2, ..., d\}$ are independent Gaussian white noises, as defined in (13).

Several questions remain about the implementation of this approximation in algorithmic form. How do we choose the parameters of the simulation? How does the choice of these parameters effect the number Q_L of random weights necessary to compute the random field $v^T(\cdot)$ locally (at a point)? What is the number Q_G of weights and convolutions necessary to compute the field globally (at all points in the domain)? How do we compute the random variables and convolutions required for this algorithm? All of these questions were discussed for the multiwavelet expansion of a simple shear field in [8], and many of the details of the implementation remain the same for multiple shear fields as for a single shear field. Therefore, in the next section we give coherent, if not entirely self-contained, answers to these questions concentrating on new features and streamlined explanations below. The reader who is willing to accept the fact that there are computational strategies for the generation of the random weights requiring little time and memory can proceed immediately to the numerical results in Section 4.

3. PARAMETER CHOICE AND ALGORITHMIC EFFICIENCY

Before we describe our procedure for choosing parameters in (35), we must restrict the domain of the field $v^T(\cdot)$ so that the number of random weights required to simulate the field is finite. With this restriction, we calculate the number Q_L of random weights required to generate the field locally, the number Q_G required to simulate the random field globally, and an index function $q(\cdot)$ which assigns independent standard Gaussian random variables from a sequence $\{g(n) | n = 0, 1, ...\}$ to the random weights $N_{rs}(\phi_{mn}^{\sigma\tau})$. Finally, we use this index to transform (35) to a Monte Carlo algorithm and discuss the choice of parameters for this algorithm and the effects of parameter choice on efficiency.

Although for a fixed $\mathbf{x} \in \mathbb{R}^d$ the expansion of $v^T(\mathbf{x})$ in (35) involves only finite sums, the number of random variables necessary to generate the entire field as $\mathbf{x}$ ranges over $\mathbb{R}^d$ is infinite. Therefore, we must restrict the domain of $v^T(\mathbf{x})$ to the open ball of radius ρ about the origin, i.e., $\{\mathbf{x} | \ |\mathbf{x}| < \rho\}$, to ensure that the number Q_G of random weights required to simulate one realization of the random field $v^T(\mathbf{x})$ will be finite. The restriction $|\mathbf{x}| < \rho$ means that each plane wave $\tilde{v}^r(x)$ need only be simulated for x in the interval (x_0, x_1), where $x_1 - x_0 = 2\rho$ and the choice of x_0 is arbitrary. Under these restrictions the number Q_G of random variables required to generate a realization of the field $v^T(\mathbf{x})$ is finite.

We count the random weights required in the expansion of $v^T(\mathbf{x})$. Because of the limitations in the range of x, indices of the random weight $N_{rs}(\phi_{mn}^{\sigma\tau})$ have finite ranges given by

$$r = 1, 2, ..., M \quad (36a)$$

$$s = 1, 2, ..., d \quad (36b)$$

$$m = m_0, ..., m_1 \quad (36c)$$

$$n = \lfloor 2^m x_0 \rfloor - b, ..., \lfloor 2^m x_1 \rfloor + b \quad (36d)$$

$$\sigma = 1, 2, ..., \tau. \quad (36e)$$

As noted above, r is the plane wave index, s is the coordinate index, m is the octave number, n is the translate, and σ is the wavelet index. From the limits on n in (36d) we see that for

fixed r,s, and σ and for m satisfying $p_0 \le m \le p_1$, the number of random weights $N_{rs}(\phi_{mn}^{\sigma\tau})$ is determined by

$$C(p_0, p_1; x_0, x_1) = (2b + 1)(p_1 - p_0 + 1) + \sum_{k=p_0}^{p_1} \lfloor 2^k x_1 \rfloor - \lfloor 2^k x_0 \rfloor. \tag{37}$$

Using this count of random weights between two octaves, we see that the number Q_L of random weights required for a single point evaluation and the number Q_G required for an entire realization are given by the equations

$$Q_L = M\, d(2b + 1)(m_1 - m_0 + 1)\, \tau \tag{38a}$$

$$Q_G = M\, dC(m_0, m_1; x_0, x_1)\, \tau, \tag{38b}$$

where M is the number of plane wave directions, d is the dimension of the space, $C(m_0, m_1)$ is defined in (37), and τ is the order of the Alpert–Rokhlin multiwavelet.

We define the indexing function $q(\cdot)$ and use an independent standard Gaussian sequence $g(\cdot)$ indexed by $q(\cdot)$ to represent these random weights. Using the ranges for the indices defined in (36), we define $q(\cdot)$ as

$$q(r, s, m, n, \sigma) = \sigma \tag{39a}$$

$$+ \tau(n - \lfloor 2^m x_0 \rfloor + b) \tag{39b}$$

$$+ \tau C(m_0, m - 1; x_0, x_1) \tag{39c}$$

$$+ \tau(s - 1)\, C(m_0, m_1; x_0, x_1) \tag{39d}$$

$$+ \tau(r - 1)\, dC(m_0, m_1; x_0, x_1). \tag{39e}$$

The linear index $q(\cdot)$ maps the ordered sets of indices (r, s, m, n, σ) onto $\{0, 1, \ldots, Q_G - 1\}$ in increasing lexicographic order with r being the most significant index. Therefore, if $\{g(n) | n = 0, 1, \ldots\}$ is an independent sequence of Gaussian random variables with zero mean and unit variance, then

$$N_{rs}(\phi_{mn}^{\sigma\tau}) = g(q(r, s, m, n, \sigma)) \tag{40}$$

in the sense that both sides of the equality have the same joint distributions as the indices r, s, m, n, and σ range over the values in (36).

Now, we use the index that we have derived to transform (35) into an algorithm. Using the formula in (40) and the notation.

$$K_s(x; m, n, \sigma) = (G_s * \phi_{mn}^{\sigma\tau})(x)$$

we transform the equations for the expansion from (35)

$$v^T(\mathbf{x}) = \sum_r U^*(\omega_r)\tilde{v}_r(\mathbf{x} \cdot \omega_r)$$

$$\tilde{v}_r(x) = \sum_s \sum_{m=m_0}^{m_1} \sum_{n=\lfloor 2^m x \rfloor - b}^{\lfloor 2^m x \rfloor + b} \sum_\sigma (G_s * \phi_{mn}^{\sigma\tau})(x) N_{rs}(\phi_{mn}^{\sigma\tau}) e_s$$

to the expression

$$v^T(\mathbf{x}) = \sum_r U^*(\omega_r)\tilde{v}_r(\mathbf{x} \cdot \omega_r + x_0 + \rho) \tag{41a}$$

$$\tilde{v}_r(x) = \sum_{smn'\sigma} K_s(x; m, \lfloor 2^m x \rfloor + n', \sigma)\, g(q(r, s, m, \lfloor 2^m x \rfloor + n', \sigma)) e_s, \tag{41b}$$

where the index ranges are given in (36). Equation (41) defines a usable algorithm for the simulation of the stationary, isotropic Gaussian random field $v^T(\cdot)$.

We could use the indexing scheme in (41) to recall the Gaussian random variables from an array $g(\cdot)$; instead, we will use the index to *compute* the Gaussian random variables. This has the advantage that memory restrictions are not a concern in generating random fields which are accurate over many scales; moreover, since the random weights are generated in a small constant amount of time, our implementation is asymptotically efficient. We defer to Section 3.1 the description of our technique for generating pseudo-random Gaussian variables on demand for the algorithm described by (41).

Finally, we can describe the choice of parameters for the algorithm in (41); this choice procedure is specific to the case of the power-law spectrum. The selection of the number M of shearing directions has been discussed in Section 2.1.2. We are *content with an isotropy tolerance* η *of approximately 1% (see* (22)) so that we choose 32 shearing directions in accordance with Table I. We choose the remaining parameters to obtain the maximum range of scales representable in floating point arithmetic with a 52-bit mantissa so that $m_1 - m_0 + 1 \le 52$. The remaining parameters are the radius ρ of the domain of $v^T(\cdot)$, the domain (x_0, x_1) of each plane wave $\tilde{v}(x)$, the minimum and maximum octaves of the expansion m_0 and m_1, respectively, and the order τ of the Alpert–Rokhlin multiwavelet and the bandwidth b.

Because we are simulating a power-law random field, the plane wave field can be scaled

$$\tilde{v}_r(x) = \lambda^{1-\varepsilon/2}\tilde{v}_r(\lambda x),$$

for $\lambda > 0$ in the sense that both sides have the same finite-dimensional distributions. Since the overall scale is arbitrary, we choose ρ arbitrarily. Since the plane waves are stationary, we choose x_0 arbitrarily; however, we need to satisfy the equation $x_1 - x_0 = 2\rho$.

Our experience in [8] leads us to choose the octave range, $m_0 \le m \le m_1$ according to the maximum and minimum length

scales, λ_1 and λ_0, that we wish to resolve. The support of the largest wavelet in the expansion is 2^{-m_0} and should be $2^{10}\lambda_1$ or more. The support of the smallest wavelet in the expansion is 2^{-m_0} and should be $2^{-3}\lambda_0$ or less. These rules ensure that the bias in simulating the structure function with a finite octave expansion in (41) will be no more than about 1%. Since the computational cost Q_L (see (38)) is linear in the number of scales, the inclusion of an "extra" 13 octaves does not appreciably contribute to the running time of our algorithm. Because the usual representation of a double precision floating point number has a 52-bit mantissa, we limit the octave range by $m_1 - m_0 + 1 \leq 52$. (Although the Cray C90 uses a larger mantissa, we did not take advantage of this because we wanted our results to be reproduceable on workstations.)

If we fix the m_0 and m_1 in the truncated expansion of $v^T(\mathbf{x})$ and compute the variance as a function of the bandwidth b in the sum, then the variance converges as b tends to infinity. If $V(b)$ is the variance as a function of b, then

$$\frac{V(\infty) - V(b)}{V(\infty)} = O(b^{\varepsilon - 2(\tau+1)}), \tag{42}$$

where τ is the order of the Alpert–Rokhlin multiwavelet and ε is the index of the spectrum $E(k) = |k|^{1-\varepsilon}$ (see [8]). The tolerance described by (42) provides a criterion for choosing b given τ. We choose the tolerance in (42) to be less than 10^{-9}.

Still remaining are the issues of computing convolutions and random weights in (41). For numerically stable formulas for computing these convolutions, the reader should consult [8]. Our somewhat involved technique for calculating random weights without using a significant amount of memory is the subject of Section 3.1. By assuming that the generation of random weights on demand requires little time or memory, some readers can go directly to the numerical results in Section 4 in a first reading.

3.1. Random Variate Generation

The most commonly used technique for generating a nearly independent pseudorandom standard Gaussian sequence $\{g(n)\}$ is to generate a uniformly distributed sequence $\{w(n)\}$ and to map $\{w(n)\}$ to $\{g(n)\}$. The sequence $\{w(n)\}$ is usually defined by a recurrence relation

$$w(0) = w, \tag{43a}$$
$$w(n) = f(w(n-1)), \tag{43b}$$

where w is any element the set S, which is assumed to have c elements and f is a permutation on S, e.g., a linear congruential generator (see [16]). The set S is the collection of *seeds* and the function f a *generator.* Usually, f is chosen so that the sequence $\{w(n)\}$ has cycle length c; this causes the distribution of $\{w(n)\}$ to be uniform on S. We refer to such a generator as a *maximally cyclic* generator.

For our purposes the number of sequence elements Q_G (see (37b)) in a realization is quite large, between 2^{49} and 2^{50}, so that we can neither generate nor store all the sequence elements for the random weights. Therefore, we generate the elements of the sequence $\{g(n)\}$ as needed. So, we write the recurrence (39) as

$$W(n) = f^n(w)$$

so that we can jump to any element of the sequence $\{w(n)\}$ by applying the appropriate power of f. If we let $\gamma(\cdot)$ refer to the transformation from $w(n)$ to $g(n)$ and denote $f^n(w)$ by

$$f^n(w) = [n]_f w, \tag{44}$$

then the set of Gaussian weights in (41) can be written in terms of powers of f as

$$g(q(r, s, m, \lfloor 2^m x \rfloor + n', \sigma)) = \gamma([q(r, s, m, \lfloor 2^m x \rfloor + n', \sigma)]_f w). \tag{45}$$

To exploit this formula we use some of the algebraic properties of generators.

A collection F of *generators* is a subgroup of the permutation group on the set of seeds $S = s_1, s_2, \ldots, s_c$. That is to say that all elements of F map S onto S and that for any $f, g, h \in F$ there are unique generators $e, f^{-1} \in F$ satisfying

$$\begin{aligned} f(gh) &= (fg)h \\ fe &= ef \\ &= f \\ ff^{-1} &= f^{-1}f \\ &= e. \end{aligned} \tag{46}$$

The elements e and f^{-1} are the *identity* of F and the *inverse* of f, respectively. We require that the product of any pair of generators f and g can be computed arithmetically in a small constant number of arithmetic operations. Therefore, the nth power of any generator f can be computed in $O(\log(n))$ time. Using the bracket notation $f^n = [n]_f$ the fast power computation formula is given by the recurrence

$$\begin{aligned} [0]_f &= e \\ [n]_f &= [n/2]_f^2 [n \bmod 2]_f, \end{aligned} \tag{47}$$

where $n/2$ denotes integer division. Examples of suitable generators with these group properties are random vector generators, multiterm recurrence generators, shift register generators, and linear congruential generators. All of these techniques except the last produce sequences with cycle lengths that are independent of computer word size. Nevertheless, we use a linear congruential generator because of the simplicity of its implementation and because we have access to machines with 64-

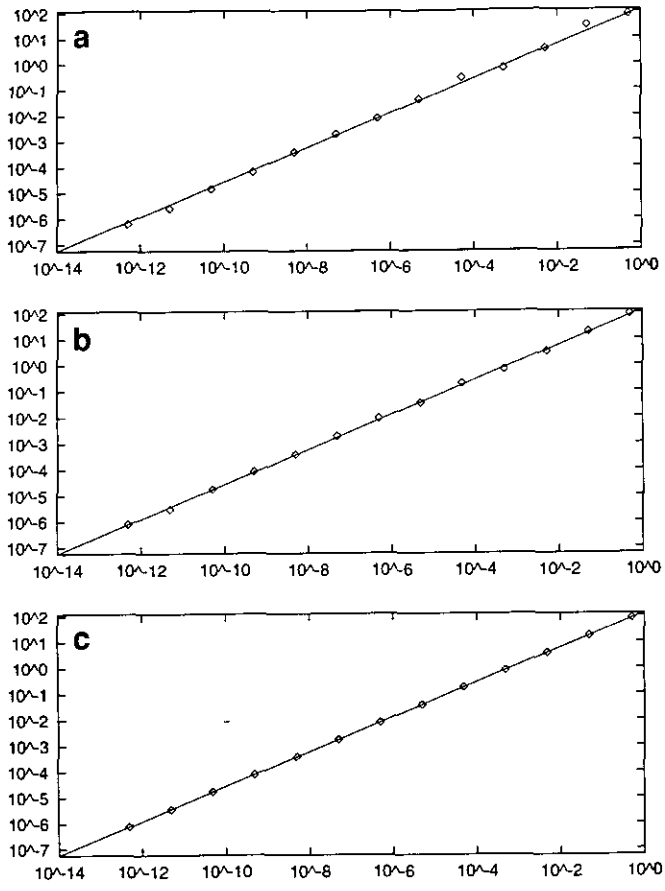

FIG. 1. Velocity structure function vs separation distance x along the ray with angle $\pi/32$ radians for a 32-plane-wave, 52-octave field. Monte Carlo statistics for (a) 10, (b) 100, and (c) 1000 realizations are plotted with the symbol ◇. The analytic value, $122.625|x|^{2/3}$ (see (25)), is plotted with a solid line.

bit word size. The *linear congruential generators* (see [17, 16]), are determined by

$$\begin{aligned} S &= \{0, 1, \ldots, c-1\} \\ F &= \{(f_0, f_1) | f_0, f_1 \in S \gcd(f_1, c) = 1\} \\ f(w) &= (f_1 w + f_0) \bmod c \\ e &= (0, 1) \\ f_g &= ((f_1 g_0 + f_0) \bmod c, (f_1 g_1) \bmod c), \end{aligned} \tag{48}$$

where $\gcd(m, n)$ is the greatest common divisor of m and n. We use a maximally cyclic linear congruential generator with $c = 2^{64}$ on a machine with 64-bit register arithmetic. Therefore, the power computation described by (47) is quite rapid for a serial computation because every stage of the recurrence requires only four multiplications and two additions. However, the necessity to perform $O(\log(n))$ *recursive* computations for each power inhibits vectorization.

We are now ready to show how to compute (45) for the random weights in a small constant amount of time and space for each weight. In (45) the index $q(\cdot)$ is given in a local form,

$$q(r, s, m, \lfloor 2^m x \rfloor + n', \sigma) = \sigma \tag{49a}$$
$$+ \tau(\lfloor 2^m x \rfloor + n' - \lfloor 2^m x_0 \rfloor + b) \tag{49b}$$
$$+ \tau C(m_0, m-1; x_0, x_1) \tag{49c}$$
$$+ \tau(s-1)\, C(m_0, m_1; x_0, x_1) \tag{49d}$$
$$+ \tau(r-1)\, dC(m_0, m_1; x_0, x_1). \tag{49e}$$

Observing that the bracket operation defined in (44), preserves sums, i.e., $[m+n]_f = [m]_f[n]_f$, we raise the generator f to the power of the index in (49) to obtain the equation

$$[q(r, s, m, \lfloor 2^m x \rfloor + n', \sigma)]_f = [\sigma]_f \tag{50a}$$
$$\times [\lfloor 2^m x \rfloor]_{f^\tau} \tag{50b}$$
$$\times [n']_{f^\tau} \tag{50c}$$
$$\times [C(m_0, m-1; x_0, x_1) - \lfloor 2^m x_0 \rfloor]_{f^\tau} \tag{50d}$$
$$\times [(s-1)\, C(m_0, m_1; x_0, x_1)]_{f^\tau} \tag{50e}$$
$$\times [(r-1)\, dC(m_0, m_1; x_0, x_1)]_{f^\tau}. \tag{50f}$$

Each term (50a) through (50f) is dependent on a single variable, and only the variable $\lfloor 2^m x \rfloor$ in term (50) assumes a large number of values. Therefore, the values of terms (50a), (50c), (50d), (50e), and (50f) can be precomputed for each σ, n', m, s, and r, respectively, and stored in five arrays. Term (50b) is problematic because if the field is to be represented over a large range of scales then term (50b) can assume more values than can be stored in any computer.

However, term (50b) can be computed recursively in m. Consider the definitions of the integer part T and the fractional part F of $2^m x$,

$$\begin{aligned} T(m, x) &= \lfloor 2^m x \rfloor \\ F(m, x) &= 2^m x - \lfloor 2^m x \rfloor. \end{aligned} \tag{51}$$

The value of term (50b) is $[T(m, x)]_{f^\tau}$. The recursive formulas for the integer part and the fractional part of $2^m x$,

$$\begin{aligned} T(m_0, x) &= \lfloor 2^{m_0} x \rfloor \\ T(m, x) &= 2T(m-1, x) + \lfloor 2F(m-1, x) \rfloor \\ F(m_0, x) &= 2^{m_0} x - \lfloor 2^{m_0} x \rfloor \\ F(m, x) &= 2F(m-1, x) - \lfloor 2F(m-1, x) \rfloor, \end{aligned} \tag{52}$$

give a recursive formula for $[T(m, x)]_{f^\tau}$,

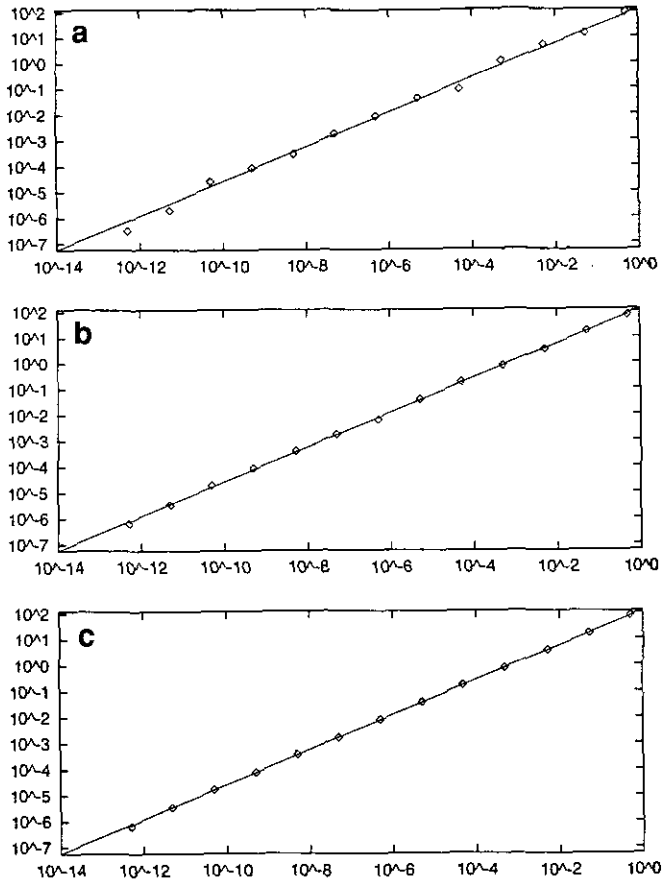

FIG. 2. Velocity structure function vs separation distance along the ray with angle $17\pi/32$ radians (see Fig. 1).

$$[T(m_0, x)]_{f^\tau} = [\lfloor 2^{m_0} x \rfloor]_{f^\tau}$$
$$[T(m, x)]_{f^\tau} = [T(m-1, x)]^2_{f^\tau} \times [\lfloor 2F(m-1, x) \rfloor]_{f^\tau}. \tag{53}$$

If we perform the summation in the algorithm (see (41)) in increasing m, we need only store $[T(m-1, x)]_{f^\tau}$, $F(m-1, x)$, and f^τ to compute $[T(m, x)]_{f^\tau}$. By carefully ordering the summation in (41) we ensure that the recursion in the computation of $[T(m, x)]_{f^\tau}$ does not depend on data already in the processor pipeline. Therefore, the computation of all random weights by the equation

$$N_{rs}(\phi^{\sigma\tau}_{mn}) = \gamma([q(r, s, m, \lfloor 2^m x \rfloor + n', \sigma)]_f s),$$

for $n = \lfloor 2^m x \rfloor + n'$, is *fully vectorizable*. Apart from minor optimizations, we computed the random weights for the algorithm as described.

4. NUMERICAL RESULTS

We simulated a two-dimensional, incompressible, stationary, isotropic, gaussian velocity field $v(\cdot)$ with radial energy spectrum

$$E(k) = 2|k|^{1-\varepsilon}$$

with $\varepsilon = \frac{8}{3}$, the value associated with the inertial range spectrum for the Kolmogoroff theory of turbulence, using the random plane wave algorithm described in Sections 2 and 3. With the criteria in Section 3.2.1, we made the following parameter choices for generating $v^T(\cdot)$ as specified in (35):

$$\begin{aligned} \rho &= 1 \\ M &= 32 \\ d &= 2 \\ x_0 &= 0, \qquad x_1 = 2 \\ m_0 &= -11, \qquad m_1 = 40 \\ \tau &= 4 \\ b &= 3. \end{aligned} \tag{54}$$

Here we recall that ρ is the radius of the domain of $v^T(\mathbf{x})$, (x_0, x_1) is the domain of the plane wave, M is the number of

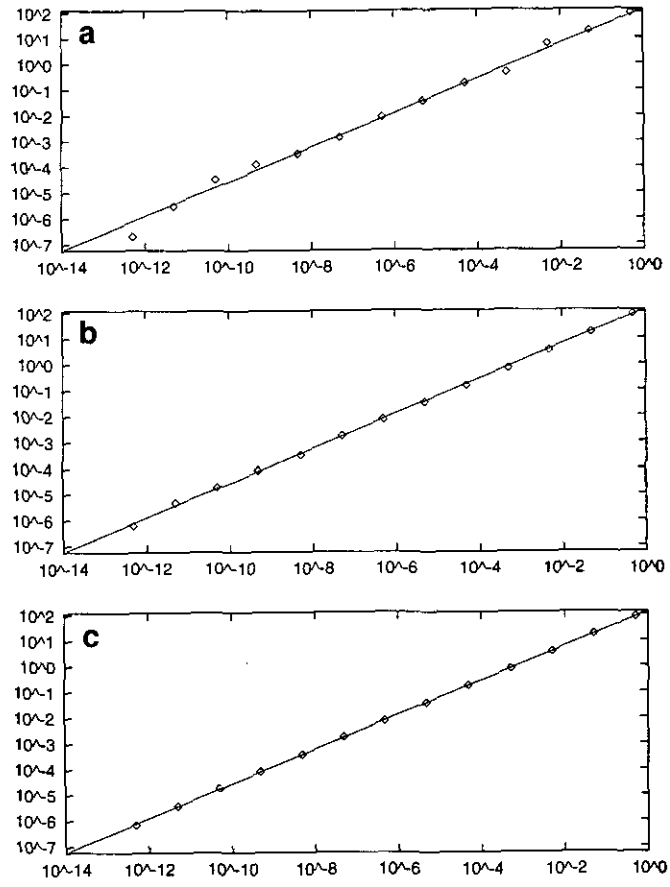

FIG. 3. Velocity structure function vs separation distance along the ray with angle $33\pi/32$ radians (see Fig. 1).

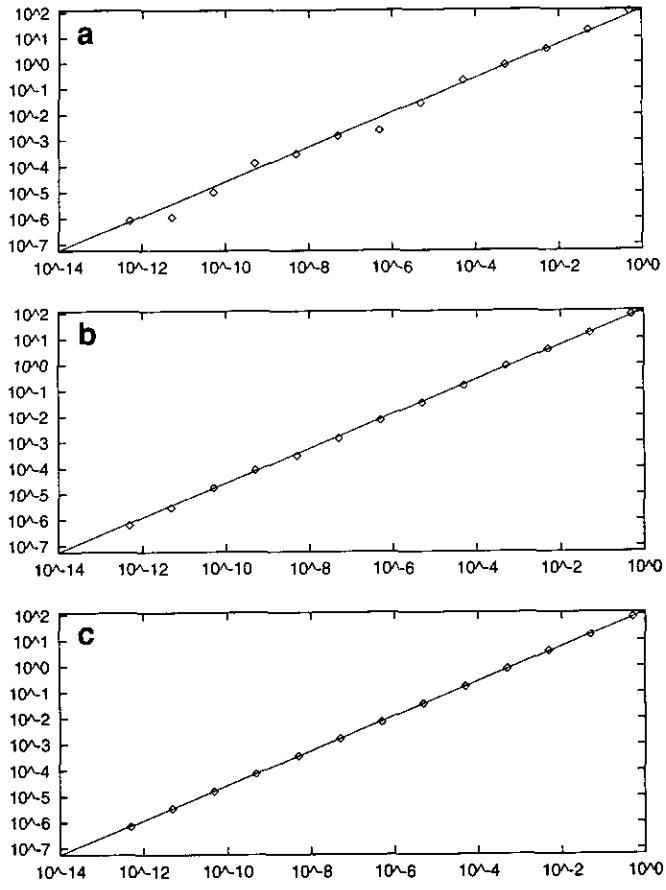

FIG. 4. Velocity structure function vs separation distance along the ray with angle $49\pi/32$ radians (see Fig. 1).

lane wave directions, d is the number of dimensions, the octave range is m_0 to m_1, and b is the bandwidth. All simulations were performed with 32 shearing directions and 52 octaves of multiwavelets per shear field. The choice of 32 shear directions was motivated by the analysis in Section 2.1.2, which is summarized in Table I. The local and global number of random variables required to generate the field with these parameters are given by

$$Q_L = 2^5 \times (2 \times 3 + 1) \times 52 \times 4$$
$$Q_G = 2^5 \times (10 + 2^{42} + 2 \times 3 \times 52) \times 4,$$

where Q_L and Q_G are given in (38). With this field we performed several tests of scaling, stationarity, and isotropy. With these parameters the algorithms require 46,592 active elements needed in the representation. Nevertheless, we will demonstrate below high accuracy with low variance for this method over 12 decades of scaling.

We conducted two tests of our simulation of the random field $v^T(\cdot)$. The first was a test of scaling properties of the trace and eigenvalues as the angle varied over five directions and the scale varied over 12 decades. These results are summarized in Figs. 1 through 5 and Tables II through IV. The second test was a test of isotropy and stationarity of two point statistics in which several pairs of points in the field were chosen at random and structure tensors were computed for each point pair. The results of this test are summarized in Fig. 6 and Tables V and VI.

We investigate the scaling properties of the simulated field. Figures 1–5 are log–log plots of the structure function (the trace of the structured tensor)

$$\text{Trace}(D_{11}(x)) = \langle |v(x) - v(0)|^2 \rangle$$

as $|x|$ varies from 0.5 to 0.5×10^{-13} in powers of 10 (within each figure) and as the angle of x assumes values of $\pi/32$, $17\pi/32$, $33\pi/32$, $49\pi/32$, and $\pi/16$ in Figs. 1–5, respectively. (We did not make the largest value of $|x|$ equal to 1 because our method implements $v^T(\cdot)$ on the *open* unit disk.) Parts a, b, and c of each figure show the predicted value of the trace graphed with simulated values of trace with sample sizes of 10, 100, and 1000, respectively. In all plots the simulated values

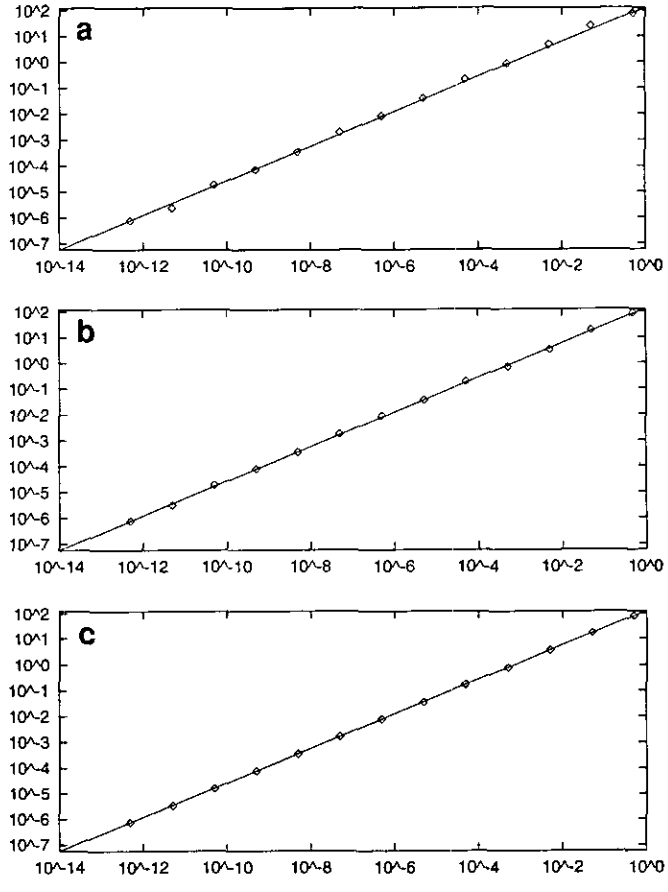

FIG. 5. Velocity structure function vs separation distance along the ray with angle $\pi/16$ radians. This ray is in the same direction as one of the plane waves (see Fig. 1).

of the trace closely followed the $\varepsilon - 2 = \frac{2}{3}$ scaling law. As Table II indicates, the error in the least-squares fit of the exponent of the trace of the structure function is never more than 3.3% for a sample size of 10. This error does not exceed 1.1% for a sample size of 100 and is never more than 0.4% for a sample size of 1000 over the entire 12 decades of scaling range. The prefactor of this scaling law is a more sensitive statistical test. From Table II the error in the least-squares fit of the coefficient is never more than 37% for a sample size of 10, never more than 6.0% for a sample size of 100, and never more than 5.0% for a sample size of 1000.

Tables III and IV present least-squares fits of the Monte Carlo simulated eigenvalues of the velocity structure tensor (see Eqs. (9), (10), and (11)). This is a much more sensitive test of the accuracy of the field than the trace alone. Recall from (25) and the formula below (27) that for two space dimensions, $d = 2$, the parallel eigenvalue is smaller so that its estimation represents a severe test. This accounts for the slightly erratic behavior of the parallel eigenvalue which we find in our numerical tests. As the tables indicate, the errors in the least-squares fit of the exponents for both eigenvalues of the structure function is never more than 6.5% for a sample size of 10, never more than 1.1% for a sample size of 100, and never more than 0.6% for a sample size of 1000 over the 12-decade range. Again, the estimates of the coefficients show much more error. For a sample size of 10 the maximum coefficient error is about 55%, occurring in the coefficient of the parallel eigenvalue. For a sample size of 100 the coefficient error for both eigenvalues is always less than 24%. For a sample size of 1000 the coefficient error in the parallel eigenvalue is as large as 8.7% though more typically about 3%; this reflects a bias caused by sampling only 32 shear directions as Table I predicted. The error in the coefficient in the perpendicular eigenvalue shows no such systematic error, and the maximum error is about 2.7%.

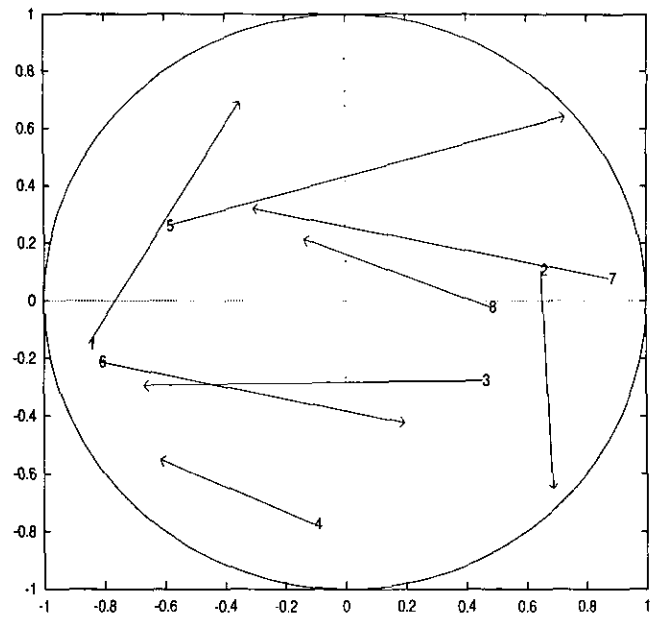

FIG. 6. Schematic diagram of random point pairs for Tables V and VI which give the rotated and scaled velocity structure tensors (see (25)) for these point pairs with 100 and 1000 samples, respectively.

TABLE II

Fits of Trace

Angle	Sample size	Coefficient	Power	Coeff. err. percentage	Power err. percentage
$\pi/32$	10	168.840	0.685	37.688	2.795
$\pi/32$	100	129.937	0.668	5.963	0.247
$\pi/32$	1000	124.684	0.667	1.679	0.113
$17\pi/32$	10	154.482	0.685	25.979	2.734
$17\pi/32$	100	122.385	0.666	−0.196	−0.080
$17\pi/32$	1000	128.717	0.669	4.968	0.371
$33\pi/32$	10	154.214	0.683	25.761	2.463
$33\pi/32$	100	116.011	0.665	−5.394	−0.319
$33\pi/32$	1000	124.830	0.667	1.798	0.111
$49\pi/32$	10	143.959	0.688	17.398	3.228
$49\pi/32$	100	127.293	0.673	3.807	1.011
$49\pi/32$	1000	124.290	0.669	1.358	0.294
$\pi/16$	10	159.228	0.680	29.849	1.945
$\pi/16$	100	128.778	0.668	5.018	0.261
$\pi/16$	1000	123.276	0.668	0.531	0.167

TABLE III

Fits of Parallel Eigenvalue

Angle	Sample size	Coefficient	Power	Coeff. err. percentage	Power err. percentage
$\pi/32$	10	58.501	0.687	27.220	2.998
$\pi/32$	100	43.111	0.665	−6.249	−0.216
$\pi/32$	1000	47.512	0.669	3.321	0.341
$17\pi/32$	10	63.406	0.694	37.885	4.161
$17\pi/32$	100	56.925	0.674	23.791	1.090
$17\pi/32$	1000	50.000	0.671	8.732	0.587
$33\pi/32$	10	56.811	0.694	23.544	4.136
$33\pi/32$	100	42.418	0.664	−7.756	−0.391
$33\pi/32$	1000	47.153	0.669	2.540	0.311
$49\pi/32$	10	71.391	0.709	55.251	6.409
$49\pi/32$	100	45.657	0.672	−0.712	0.766
$49\pi/32$	1000	46.876	0.668	1.939	0.255
$\pi/16$	10	59.418	0.687	29.214	3.059
$\pi/16$	100	43.668	0.666	−5.038	−0.030
$\pi/16$	1000	47.094	0.670	2.413	0.524

The second test was conducted by choosing eight pairs of points uniformly and independently on the unit disk. For this test we reduced m_1 to 29 since accuracy over a large range of scales was unimportant for this test and since this modification reduced the running time. All other parameters are as they appear in (54). Figure 6 depicts these point pairs with arrows connecting them. The lengths of the arrows varied from 0.56 to 1.38. The value of the field at the tail of each arrow was subtracted from the value of the field at the head of the arrow, and statistics were calculated for the components of this difference parallel to and perpendicular to each arrow. In accordance with the formula in (24), the

TABLE IV

Fits of Perpendicular Eigenvalue

Angle	Sample size	Coefficient	Power	Coeff. err. percentage	Power err. percentage
$\pi/32$	10	106.994	0.684	39.605	2.643
$\pi/32$	100	86.310	0.670	12.617	0.474
$\pi/32$	1000	77.160	0.667	0.678	−0.021
$17\pi/32$	10	87.391	0.679	14.026	1.911
$17\pi/32$	100	64.873	0.660	−15.354	−1.004
$17\pi/32$	1000	78.720	0.668	2.713	0.244
$33\pi/32$	10	91.690	0.679	19.636	1.784
$33\pi/32$	100	73.126	0.665	−4.586	−0.280
$33\pi/32$	1000	77.668	0.667	1.341	−0.005
$49\pi/32$	10	69.661	0.677	−9.107	1.533
$49\pi/32$	100	80.547	0.674	5.097	1.115
$49\pi/32$	1000	77.320	0.669	0.887	0.315
$\pi/16$	10	95.106	0.674	24.094	1.108
$\pi/16$	100	84.800	0.670	10.646	0.457
$\pi/16$	1000	76.167	0.666	−0.618	0.042

TABLE V

Test of Isotropy with Sample Size 100

Pair	$\lambda_\parallel$	$\lambda_\perp$	$\text{Flat}_\parallel$	$\text{Flat}_\perp$	$\lambda_\parallel$ err. percentage	$\lambda_\perp$ err. percentage	$\text{Flat}_\parallel$ err. percentage	$\text{Flat}_\perp$ err. percentage
1	38.5	96.3	2.08	4.99	−16.20	25.66	−30.75	66.27
2	60.3	69.9	5.04	1.82	31.11	−8.74	67.99	−39.33
3	41.7	69.6	2.49	2.48	−9.28	−9.18	−17.08	−17.34
4	41.0	91.5	2.35	3.59	−10.87	19.35	−21.62	19.74
5	43.0	73.0	3.08	3.00	−6.45	−4.78	2.79	−0.03
6	43.1	73.6	2.86	3.26	−6.24	−3.94	−4.68	8.81
7	44.5	48.9	2.90	1.27	−3.25	−36.23	−3.29	−57.54
8	54.6	58.6	5.14	1.53	18.78	−23.54	71.37	−49.05
Exact	46.0	76.6	3.00	3.00				

field components were multiplied by the length of the arrow to the power $\varepsilon/2 - 1$, and the results for 100 and 1000 samples are presented in Tables V and VI. The true values of the scaled parallel and perpendicular component variances are $\lambda_\parallel = 45.984$ and $\lambda_\perp = 76.641$, respectively. The ratios of the fourth moments to the squares of their respective variances are 3 because the components are Gaussian. For a sample size of 100, the variances in the parallel and perpendicular components had errors as large as 36% although usually smaller than 20%. For the same sample the errors in flatness of each component were as large as 71% though usually smaller than 50%. For a sample size of 1000, the variances of the components had errors as large as 8.6% although usually less than 5%. For the same sample the errors in the flatness of the components were as large as 18% although usually less than 12%. Given that estimators of flatness are high variance statistics, the accuracy of the flatness statistics for the sample size of 1000 provides a reasonable confirmation that our simulated statistics were Gaussian.

These tests indicate that the multishear algorithm with 32 shear directions and a 52-octave, fourth-order Alpert–Rokhlin multiwavelet expansion for each shear field produces an excellent approximation of the true field over approximately 12 decades of scaling. The scaling properties of the field, as demonstrated in Figs. 1–5 and in Tables II–IV, are outstanding. They demonstrate the value of the rapid convergence of the multiwavelet expansion of (34) in combination with on-demand generation of random weights. The isotropy and stationarity properties are also excellent because the field is implemented in terms of random plane waves.

5. CONCLUDING REMARKS

In Sections 2 and 3 of this paper, the authors have developed a new Monte Carlo algorithm for Gaussian isotropic random fields with fractal behavior and infrared divergence. This algorithm combines a random plane wave approximation utilizing a fixed finite number of directions [12] with a recent wavelet Monte Carlo method for random fields with infrared divergence in a single space dimension ([8]). The numerical results in Section 4 demonstrate the low variance of the algorithm, where only 100 realizations (and 10 for scaling results) are needed to simulate a Gaussian random field with

TABLE VI

Test of Isotropy with Sample Size 1000

Pair	$\lambda\parallel$	$\lambda_\perp$	$\text{Flat}\parallel$	$\text{Flat}_\perp$	$\lambda\parallel$ Err. percent	$\lambda_\perp$ Err. percent	$\text{Flat}\parallel$ Err. percent	$\text{Flat}_\perp$ Err. percent
1	46.8	78.2	3.13	3.22	1.82	2.02	4.49	7.25
2	48.3	74.3	3.27	2.64	5.02	−3.02	8.87	−12.06
3	46.4	77.6	3.12	3.27	0.83	1.29	3.99	9.03
4	48.8	79.3	3.54	3.01	6.04	3.48	18.06	0.23
5	43.8	70.8	2.63	2.61	−4.67	−7.66	−12.31	−12.85
6	47.9	79.4	3.25	3.26	4.15	3.55	8.47	8.55
7	46.3	72.0	2.90	2.67	0.61	−6.01	−3.18	−11.16
8	47.0	70.1	3.44	2.47	2.21	−8.59	14.69	−17.63
Exact	46.0	76.6	3.00	3.00				

the Kolmogoroff spectrum in two dimensions over 12 decades. Furthermore, only 46,592 active elements are needed for each computation!! These results with the new algorithm are a substantial improvement over those produced recently by other standard procedures involving Fourier methods and/or successive random addition [10, 11]. It is also very difficult to generate incompressible wavelets with practical numerical control for these problems directly in two or three space dimensions [13]; the new algorithm circumvents this difficulty through the shear layer approximation while still utilizing the remarkable scaling and cancellation features of appropriate wavelets in one dimension [8].

In subsequent publications, the authors will apply this algorithm to problems in turbulent diffusion including the computation of the Richardson law for pair dispersion over many decades. Also, the algorithms in this paper will be generalized to situations involving random fields with long-range space–time correlations as well as three space dimensions. Furthermore, there is a rigorous convergence proof for the algorithm devised in this paper which will be developed elsewhere in the near future.

It is also worthwhile to mention here that the basic plane wave algorithm developed in Sections 2.1 and 2.2 above can be implemented with any other efficient Monte Carlo algorithm for simulating the random plane waves; these aspects will also be developed elsewhere in the near future.

REFERENCES

1. M. Lesieur, *Turbulence in Fluids* (Kluwer Academic, Boston, MA, 1990).
2. W. McComb, *The Physics of Fluid Turbulence* (Clarendon Press, Oxford, 1990).
3. G. Csanady, *Turbulent Diffusion in the Environment,* Geophysics and Astrophysics Monographs (Reidel, Dordrecht, 1973).
4. G. Dagan, *Annu. Rev. Fluid Mech.* **19,** 183 (1987).
5. F. Williams, "Turbulent Combustion," *The Mathematics of Combustion,* edited by J. Buckmaster (SIAM, Philadelphia, 1985), p. 97.
6. J. Feder, *Fractals* (Plenum, New York, 1988), Chaps. 9–14.
7. A. Monin and A. Yaglom, *Statistical Fluid Mechanics: Mechanics of Turbulence, Vol. II* (MIT Press, Cambridge, MA, 1975), Chap. 6, Section 12.
8. F. Elliott and A. Majda, *J. Comput. Phys.* **113,** 82 (1994).
9. K. Falconer, *Fractal Geometry* (Wiley, New York, 1990).
10. J. Viecelli and E. Canfield, *J. Comput. Phys.* **95,** 29 (1991).
11. F. Elliott, A. Majda, D. Horntrop, and R. McLaughlin, *J. Statist. Phys.,* submitted.
12. A. Majda, *J. Statist. Phys.* **75,** 1153 (1994).
13. I. Daubechies, *Ten Lectures on Wavelets* (SIAM, Philadelphia, 1992).
14. J. Doob, *Stochastic Processes* (Wiley, New York, 1953).
15. B. Alpert, Ph.D. thesis, Department of Computer Science, Yale University, December 1990 (unpublished).
16. H. Niedereitter, *Random Number Generation and Quasi-Monte Carlo Methods* SIAM, Philadelphia, 1992).
17. D. Knuth, *The Art of Computer Programming,* 2nd ed. (Addison–Wesley, Reading, MA, 1973).